Available online at www.sciencedirect.com
ScienceDirect
Journal of Power Sources 163 (2006) 223–228
JOURNAL OF POWER SOURCES
www.elsevier.com/locate/jpowsour

Short communication

Li_2O–B_2O_3–P_2O_5 solid electrolyte for thin film batteries

Kang Ill Cho [a], Sun Hwa Lee [a], Ki Hyun Cho [a], Dong Wook Shin [a,*], Yang Kuk Sun [b]

[a] *Division of Material Science and Engineering, Hanyang University, Seoul 133-791, Republic of Korea*
[b] *Division of Applied Chemical Engineering, Hanyang University, Seoul 133-791, Republic of Korea*

Received 22 September 2005; received in revised form 24 January 2006; accepted 6 February 2006
Available online 29 March 2006

Abstract

Solid-state glass electrolyte, xLi_2O–$(1-x)(yB_2O_3$–$(1-y)P_2O_5)$ glasses were prepared with wide range of composition, i.e. $x = 0.35$–0.5 and $y = 0.17$–0.67. This material system is one of the parent compositions for chemically and electrochemically stable solid-state electrolyte applicable to thin film battery. The purpose of this study is to seek the best composition among the various compositions for the deposition of thin film electrolytes. Lithium ion conductivity of Li_2O–B_2O_3–P_2O_5 glasses was characterized by ac impedance technique. The ionic conductivity of the electrolyte at room temperature increased with x and y. The maximum conductivity of this glass system was $1.6 \times 10^{-7}\ \Omega^{-1}\ cm^{-1}$ for $0.45Li_2O$–$0.275B_2O_3$–$0.275P_2O_5$ at room temperature. It was shown that the addition of P_2O_5 reduces the tendency of devitrification and increases the maximum amount of Li_2O added into glass former without devitrification.

Keywords: Lithium battery; Glass electrolyte; Electrical conductivity; Impedance; FTIR

1. Introduction

During the last two decades, lithium-based glasses have been studied extensively as electrolytes for solid-state secondary batteries. However, solid-state lithium batteries have not been widely commercialized because solid electrolyte has not completely satisfied the requirements for practical application. For practical use, solid electrolyte must have high ionic conductivity as well as chemical, thermal and electrochemical stability [1].

Although two types of solid inorganic electrolyte, crystalline and glass electrolyte, have been investigated, most of recent progresses have focused on glass electrolytes due to advantages over crystalline solid; isotropic ionic conduction, no grain boundaries, ease of fabrication, etc [2]. Lithium ion conductive glass is generally classified into two types depending on the composition of host material, i.e. oxide glass and sulfide glass.

Sulfide glasses show higher ionic conductivity of 10^{-3}–$10^{-4}\ S\ cm^{-1}$ at room temperature and a wide electrochemical window, and a high thermal stability against crystallization. But they are less stable in air by the hygroscopic nature of sulfur. Besides, some sulfide glasses appear to be unstable in contact with lithium metal [3], and have not been widely used largely because they are quite difficult to handle. Furthermore, sulfide ions may cause corrosion of the equipment during vacuum deposition process for thin-film electrolyte.

The advantages of the lithium oxide glasses are that they are less hygroscopic and more chemically stable in air. In contrary to sulfide glasses, oxide glasses do not react with electrode materials and this chemical inertness is advantageous for cycle performances of battery [4,5]. In addition to the chemical inertness, they are deposited easily by conventional PVD methods such as sputtering or thermal evaporation. The ease of thin film fabrication is a great advantage when the material is considered as a thin film battery.

However, oxide glasses show relativity low ionic conductivity in the order of 10^{7}–$10^{-8}\ S\ cm^{-1}$ at room temperature [2,4,5]. Thus, the major effort has been focused on the improvement of the ion conductivity of oxide glasses.

In this study, the oxide amorphous electrolytes in the system of Li_2O–B_2O_3–P_2O_5 have been prepared by melt-quenching method and the basic electrical property was characterized by ac impedance technique. This material system is one of the parent

* Corresponding authors. Tel.: +82 2 2220 0503; fax: +82 2 2299 3851.
E-mail address: dwshin@hanyang.ac.kr (D.W. Shin).

0378-7753/$ – see front matter © 2006 Elsevier B.V. All rights reserved.
doi:10.1016/j.jpowsour.2006.02.011

compositions for chemically and electrochemically stable solid-state electrolyte applicable to thin film battery. The purpose of this study is to seek the best composition among the various compositions of this material system, for the deposition of thin film electrolytes.

2. Experiments

Glass electrolytes with composition $x\mathrm{Li_2O}$–$(1-x)(y\mathrm{B_2O_3}$–$(1-y)\mathrm{P_2O_5})$ were prepared from reagents grade material (99% $\mathrm{Li_2CO_3}$, 98% $\mathrm{P_2O_5}$ and 95% $\mathrm{B_2O_3}$). The starting materials were mixed in proportions appropriate to form 30 g batches. Each batch was melted at 1000 °C for 6 h in Pt crucibles in an electrically heated furnace. The amorphous state of glass electrolytes were identified at room temperature by X-ray diffraction (XRD).

Pt was sputtered on both sides of the glass electrolyte as ion blocking electrodes to measure the ionic conductivities. Conductivity was measured by complex impedance method using IM6 impedance analyzer with an ac voltage of 50 mV amplitude over the frequency range of 1 Hz–1 MHz at room temperatures. The activation energy of Li^+ ionic conduction were measured by the temperature dependence of the conductivity in the temperature range of 25–200 °C.

The correlation between the structural modification of glass network and compositional variation and conductivity was characterized by FTIR. Glasses were ground, mixed with KBr in a 1:100 weight ratio and pressed into pellets to obtain the infrared spectra (IR Spectroscopy: Magna-IR 760 Spectrometer) in the range from 400 to 4000 $\mathrm{cm^{-1}}$. IR transmittance was measured first and converted to reflectance using Kramers–Kronig relationship.

3. Results and discussion

The glass forming ability of the material system studied in this work is summarized in a ternary diagram of Fig. 1. The filled circle symbols represent the compositions forming amorphous phase while diamond symbols represent the compositions showing partial or complete crystallization during air-cooling the specimen from the melting temperature of 1000 °C. From Fig. 1, one can see that the glass-forming region of $x\mathrm{Li_2O}$–$(1-x)(y\mathrm{B_2O_3}$–$(1-y)\mathrm{P_2O_5})$ system using conventional melting and quenching technique was limited to range of $x=0.47$ and $y=0.67$. The devitrification was checked by X-ray diffraction, which is shown in Fig. 2. The pattern shows that $x\mathrm{Li_2O}$–$(1-x)(0.5\mathrm{B_2O_3}$–$0.5\mathrm{P_2O_5})$ system was quenched into amorphous glass except for $x=0.5$. Glass-forming region in the system of $x\mathrm{Li_2O}$–$(1-x)(0.5\mathrm{B_2O_3}$–$0.5\mathrm{P_2O_5})$ ranges from $x=0.35$ to 0.47. At the composition of $x>0.5$, samples were partially crystalline or crystalline states. For $x=0.4$, the glass forming range spans from $y=0.17$ to 0.67.

Considering the fact that the quenching method employed in this work was air quenching, whose quenching speed is relatively slow, the glass-forming region could be slightly widened and, hence, the amount of Li added to glass former is slightly increased, if the faster quenching technique such as oil quenching or splat quenching is employed. It is worth to notice that by adding phosphorus as a glass former the glass forming ability or the resistance to the devitrification is improved compared to pure borate glasses. Phosphorus seems to extend the glass-forming region to higher $\mathrm{Li_2O}$ content.

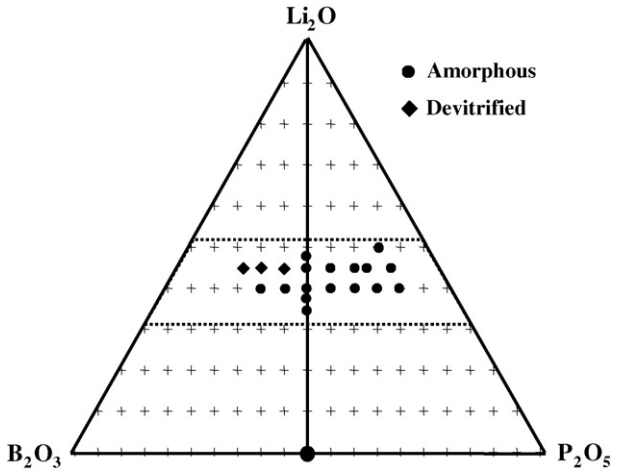

Fig. 1. The compositions of $\mathrm{Li_2O}$–$\mathrm{B_2O_3}$–$\mathrm{P_2O_5}$ ternary system studied. Filled circle and diamond symbols represent the compositions producing amorphous glass phases without (undetectable with X-ray diffraction) and with (detectable with X-ray diffraction) crystalline phases, respectively.

Fig. 3(a) shows a typical Nyquist plot of the $x\mathrm{Li_2O}$–$(1-x)(0.5\mathrm{B_2O_3}$–$0.5\mathrm{P_2O_5})$ glass system at room temperature and Fig. 3(b) presents the conductivity variation with mole fraction of network modifier, $\mathrm{Li_2O}$. As shown in Fig. 3(b), the lithium-ion conductivity of glasses is enhanced as network modifier contents increase up to $x=0.47$ due to the increase in both lithium ion concentration and non-bridging oxygen (NBO). Non-bridging oxygen site is known to offer the hoping site for ionic conduction in oxide glass network where cation such as Li^+ jumps into or out easily due to relatively weak bonding or shallow energy well [6]. The formation of non-bridging oxygen is also contributing to the relatively open network structure with large free volume for ion drift. The combination of these two effects increases the ionic conduction

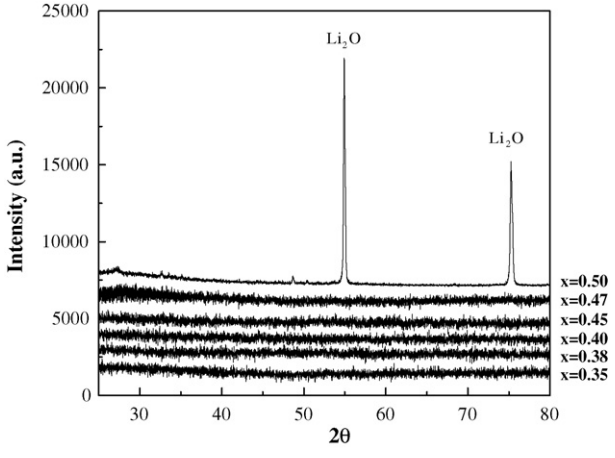

Fig. 2. X-ray diffraction pattern of $x\mathrm{Li_2O}$–$(1-x)(0.5\mathrm{B_2O_3}-0.5\mathrm{P_2O_5})$ as a function of $\mathrm{Li_2O}$ composition, x.

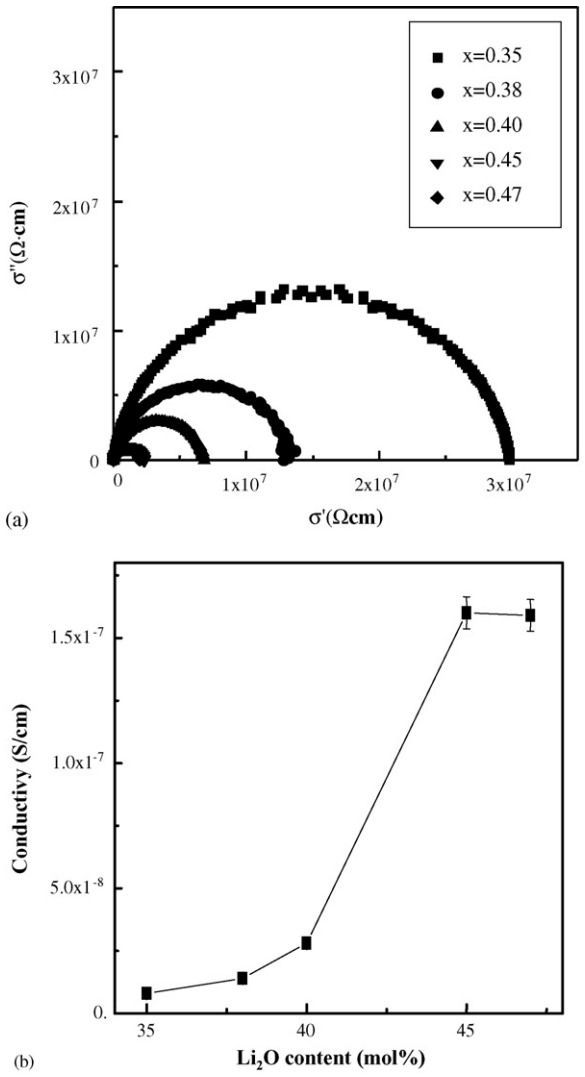

Fig. 3. The variation of conductivity of xLi$_2$O–(1−x)(0.5B$_2$O$_3$−0.5P$_2$O$_5$) glass electrolyte by the addition of Li$_2$O. (a) Typical Nyquist plots, (b) conductivity as a function of Li$_2$O concentration.

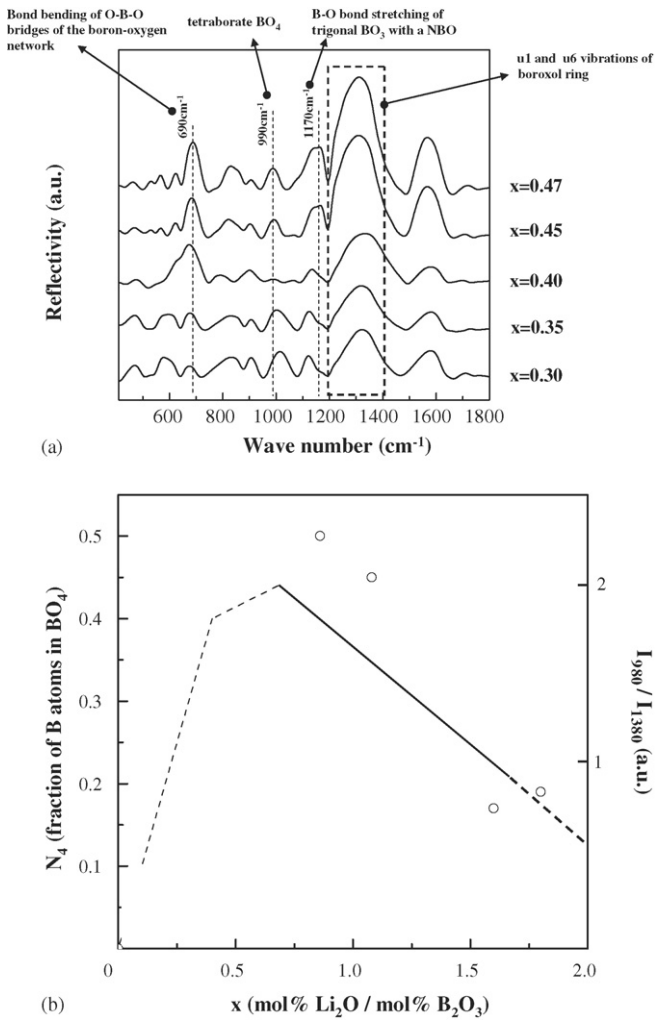

Fig. 4. The variation of FTIR spectra of xLi$_2$O–(1−x)(0.5B$_2$O$_3$−0.5P$_2$O$_5$) system glass electrolyte by the addition of Li$_2$O. (a) FTIR reflectance spectra, (b) the variation of the ratio between peak height of 990 cm^{-1} band and 1300 cm^{-1} band [7]. The peak height ratio is compared to the number of four-coordinated boron. Li$_2$O and B$_2$O$_3$ are represented in mol%.

of glass electrolyte. The variation of non-bridging oxygen content was investigated by FTIR spectra, which is summarized in Fig. 4(a). The reflectance peak around 1170 cm^{-1} is assigned to B–O bond stretching of trigonal BO_3 with a non-bridging oxygen [7]. In Fig. 4(a), one can see that this peak grows as the concentration of Li$_2$O increases. The increase of non-bridging oxygen is accompanied by the formation of BO_3 trigonal unit since, at high Li concentration, the addition of Li$_2$O converts the BO_4 tetrahedral unit to BO_3 trigonal unit with a non-bridging oxygen as described by the following equation:

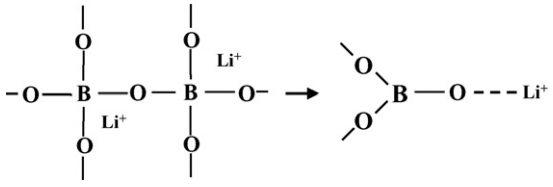

In Fig. 4(b), the fraction of four-coordinated boron is compared as a function of Li$_2$O/B$_2$O$_3$ ratio to the ratio of peak height between 990 and 1300 cm^{-1} band. The peak height ratio roughly follows the variation of four-coordinated boron which means that the relative fraction of four-coordinated boron was actually reduced dramatically as Li$_2$O concentration increased, even though the absolute peak height of 990 cm^{-1} band was not varied noticeably. This result is in good agreement with the previous report [7] that the relative fraction of trigonal BO_3 with a non-bridging oxygen increases as the concentration of Li$_2$O increases while that of four-coordinated boron reduces.

The conversion from four-coordinated boron to three-coordinated boron with a non-bridging oxygen can be also verified by the growth of the peak at 1200 cm^{-1} which is unfortunately not clear in the specimen used in this work due to large peak around 1250–1400 cm^{-1}. However, the growth of 1200 cm^{-1} peak with increasing Li$_2$O becomes apparent at high B$_2$O$_3$ concentration where the left shoulder of 1250–1400 cm^{-1} becomes taller.

Fig. 5(a) presents the conductivity variation with mole fraction of network former, B$_2$O$_3$. In this figure, the lithium-ion conductivity is enhanced as network former (B$_2$O$_3$) contents

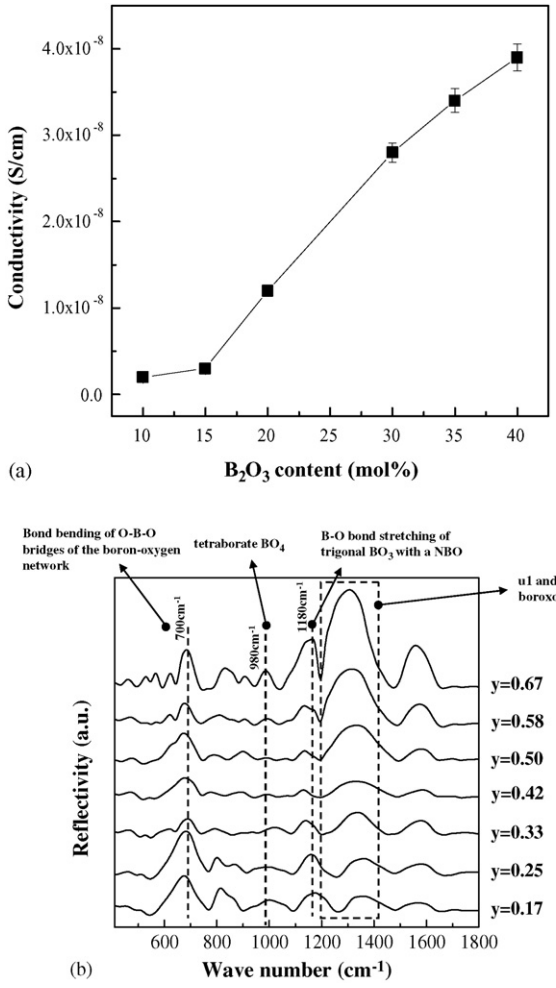

Fig. 5. The variation of conductivity and FTIR spectra of $x\mathrm{Li_2O}$–$(1-x)(y\mathrm{B_2O_3}$–$(1-y)\mathrm{P_2O_5})$ glass electrolyte at various $\mathrm{B_2O_3}$ concentration. (a) Conductivity, (b) FTIR reflectance spectra as a function of $\mathrm{B_2O_3}$ concentration.

increase up to $x = 0.4$. The increment of y or $\mathrm{B_2O_3/P_2O_5}$ ratio can be confirmed from the IR reflection peak at 1250–1400 $\mathrm{cm^{-1}}$ in Fig. 5(b) which is assigned to the harmonic vibrations of boroxol rings. The peak becomes taller since the boroxol rings become abundant as the $\mathrm{B_2O_3/P_2O_5}$ ratio increases. The peak at ~1180 $\mathrm{cm^{-1}}$, the stretching band of $\mathrm{BO_3}$ with a non-bridging oxygen, showed the minimum at $y = 0.15$ and the maximum at $y = 0.67$. This result suggests that the proportion of four-coordinated boron, $\mathrm{BO_4}$, is maximized at $y = 0.15$ or $\mathrm{B_2O_3/P_2O_5}$

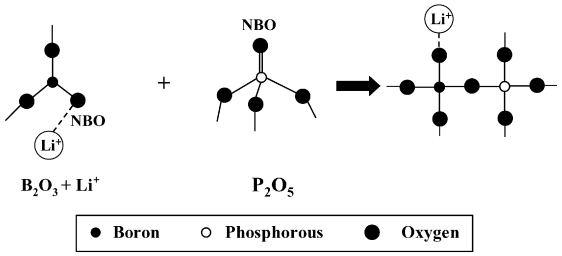

Fig. 6. The formation of four-coordinated boron by the reaction between three-coordinated boron and four-coordinated phosphorus in $\mathrm{Li_2O–B_2O_3–P_2O_5}$ glass electrolyte.

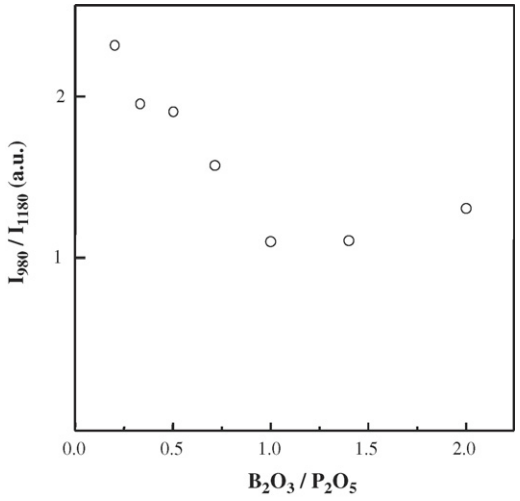

Fig. 7. The variation of ratio between peak height of 980 $\mathrm{cm^{-1}}$ band and 1180 $\mathrm{cm^{-1}}$ band shown in Fig. 5(b). $\mathrm{Li_2O}$ and $\mathrm{B_2O_3}$ are represented in mol%.

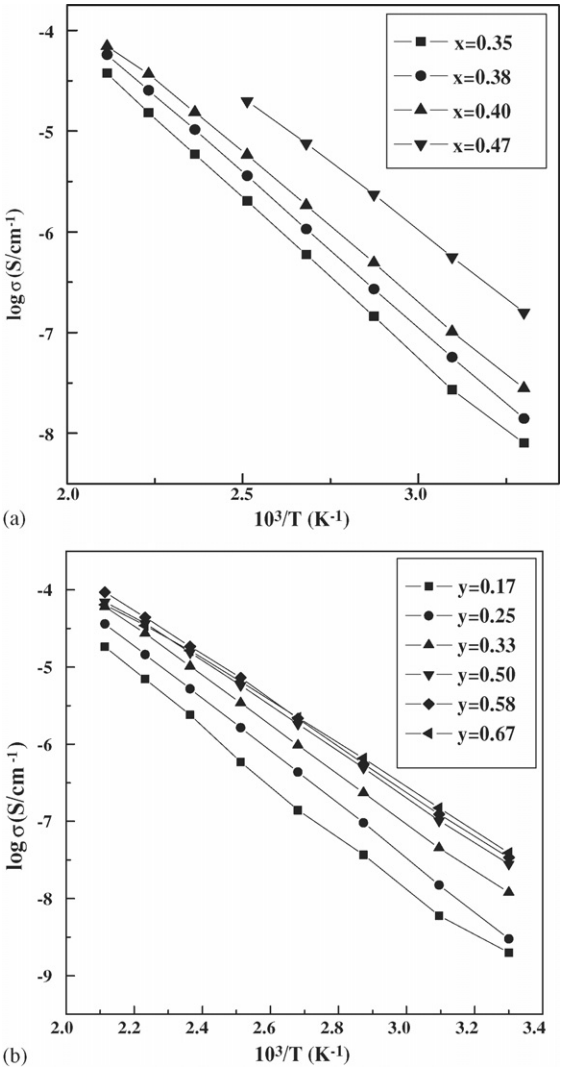

Fig. 8. The Arrehnius plots of the conductivity of $x\mathrm{Li_2O}$–$(1-x)(y\mathrm{B_2O_3}$–$(1-y)\mathrm{P_2O_5})$ glass electrolyte. The variation of temperature dependent conductivity with (a) x ($\mathrm{Li_2O}$ concentration) and (b) y ($\mathrm{B_2O_3}$ concentration).

ratio = 1. The four-coordinated boron, BO_4, is formed by the reaction depicted in Fig. 6. The non-bridging oxygen located at double bond in P_2O_5 tetrahedron easily reacts with one of BO_3 arm with a non-bridging oxygen to form two tetrahedrons and this effect would be maximized at B_2O_3/P_2O_5 ratio ≈ 1 for the statistical reason as shown in Fig. 7. Fig. 7 presents the ratio between peak height of 980 and 1180 cm^{-1} band as a function of the ratio of mole fraction of network former, B_2O_3/P_2O_5. The peak height ratio shows the minimum at $B_2O_3/P_2O_5 \approx 1$, which means that the ratio between four-coordinated boron BO_4 and three-coordinated boron BO_3 with a non-bridging oxygen is minimized at this proportion of network former.

The devitrification is closely related to the proportion of non-bridging oxygen since it weakens the glass network and lowers viscosity. The absolute amount of non-bridging oxygen in glass network increases with increasing B_2O_3 when Li_2O content is very high as in this work, and this leads to low resistance to devitrification and high electrical conductivity. The addition of P_2O_5 helps the formation of four-coordinated boron, BO_4, or reduces the concentration of non-bridging oxygen. This effect is confirmed from the conductivity data in Fig. 5(a).

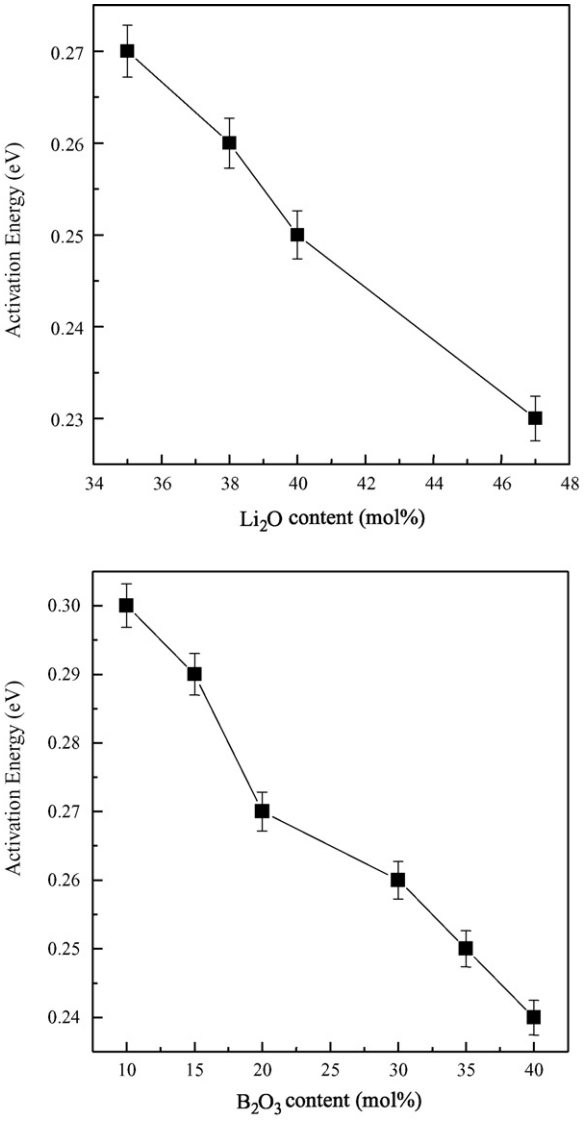

Fig. 9. The variation of activation energy of the conductivity of $x$$Li_2O$–$(1-x)$($y$$B_2O_3$–$(1-y)$$P_2O_5$) glass electrolyte. The variation of activation energy with (a) x (Li_2O concentration) and (b) y (B_2O_3 concentration).

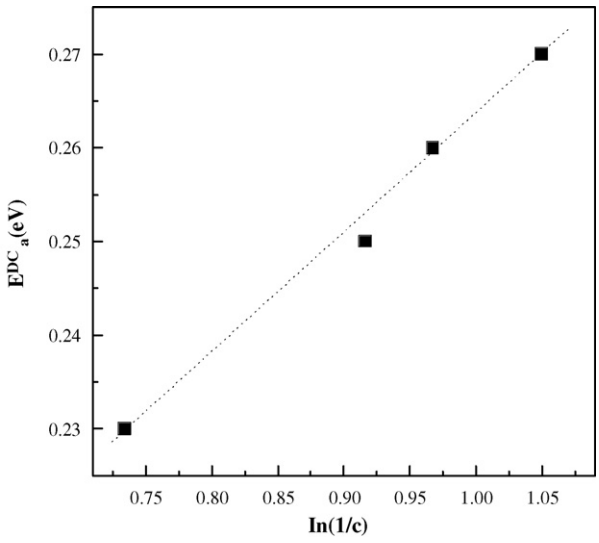

Fig. 10. Activation energy of the conductivity of $x$$Li_2O$–$(1-x)$($y$$B_2O_3$–$(1-y)$$P_2O_5$) glass electrolyte as a function of $\ln(1/c)$, where c is the concentration of ion charge carrier.

Fig. 8(a) and (b) shows the typical Nyquist plots of $x$$Li_2O$–$(1-x)$($y$$B_2O_3$–$(1-y)$$P_2O_5$) system at various temperature. For all composition, glass electrolytes show thermally activated behavior described by the following Arrhenius-type equation:

$$\sigma_{\text{ion}}^{\text{DC}} = \sigma_0 \exp\left(-E_{\text{a}}^{\text{DC}}/kT\right).$$

Here E_{a}^{DC} is the DC activation energy and σ_0 is the pre-exponential factor. The thermally activated conductivity increases with the increased temperature as shown in Fig. 8(a) and (b). From the Arrhenius plots, the room temperature DC conductivity as well as the fitted values of DC activation energy have been calculated and plotted in Fig. 9(a) and (b) as function of composition x and y. In terms of dynamic structure model, the doping effect can be explained by the activation energy decrease as ion concentration increase: $E_{\text{a}}^{\text{DC}} = \text{Const} \cdot \ln(1/c)$, where c is the ion molar concentration [8]. Our result, Fig. 10 shows activation energy has logarithmic dependence on $1/c$ up to $x = 0.47$. As the lithium concentration increase with x, activation energy is decreased, and this compositional modification is responsible for the conductivity increase [9].

4. Conclusions

Solid-state glass electrolytes, $x$$Li_2O$–$(1-x)$($y$$B_2O_3$–$(1-y)$$P_2O_5$), prepared by melt quenching method. P_2O_5 was added into binary Li_2O–B_2O_3 glass electrolyte as a network former to prevent the devitrification and help the stable formation of amorphous phase of the glass electrolyte. The addition of P_2O_5 successfully widened the glass-forming region to the regime of higher concentration of lithium.

However, the addition of P_2O_5 was not beneficial for the electrical conduction. P_2O_5 converted the three-coordinated [BO_3] with a non-bridging oxygen into four-coordinated boron eliminating non-bridging oxygen sites, which reduces the electrical conductivity of Li^+ in glass electrolyte. In other hand, as B_2O_3 contents increased, the conductivity of glass electrolyte increased due to the increase of three-coordinated [BO_3] with a non-bridging oxygen. The maximum ionic conductivity was achieved with $1.6 \times 10^{-7}\,S\,cm^{-1}$ at room temperature. The conductivity was not high enough for the application as a bulk type electrolyte. However, the conductance of this glass electrolyte can be increased by reducing the thickness of electrolyte film, the Li_2O–B_2O_3–P_2O_5 system is currently being studied in our research group as a candidate for thin film solid electrolyte and its stable glass forming ability and stable chemical properties enables the deposition under open atmosphere with the deposition technique called "aerosol flame deposition".

Acknowledgment

This work was supported by the Ministry of Information & Communications, Korea, under the Information Technology Research Center (ITRC) Support Program.

References

[1] S. Kondo, in: M. Wakihara, O. Yamamoto (Eds.), Lithium Ion Batteries: Fundamentals and Performances, Wiley-VCH, Weinheim, 1998.
[2] D. Ravaine, J. Non-Cryst. Solids 38/39 (1980) 353.
[3] J.H. Kennedy, Z. Zhang, Solid State Ionics 28–30 (1988) 726.
[4] D. Ravaine, J. Non-Cryst. Solids 38 (1980) 353.
[5] J. Akridge, H. Vourlis, Solid State Ionics 18 (1979) 1082.
[6] C.H. Lee, K.H. Joo, J.H. Kim, S.G. Woo, H.J. Sohn, T. Kang, Y. Park, J.Y. Oh, Solid State Ionics 59–65 (2002) 149.
[7] A. Krol, W. Nazarewicz, Mater. Sci. Eng. B3 (1989) 307–312.
[8] A. Bunde, M.D. Ingram, P. Maass, K.L. Ngai, J. Phys. A24 (1992) L881.
[9] K.H. Joo, P. Vinatier, B. Pecquenard, A. Levasseur, H.J. Sohn, Solid State Ionics 51–59 (2003) 160.